

See discussions, stats, and author profiles for this publication at: <https://www.researchgate.net/publication/280327197>

Theoretical Study on the Solvation of C₆₀ Fullerene by Ionic Liquids II: A DFT Analysis on the Interaction Mechanism.

ARTICLE *in* THE JOURNAL OF PHYSICAL CHEMISTRY B · JULY 2015

Impact Factor: 3.3 · DOI: 10.1021/acs.jpcb.5b03608 · Source: PubMed

CITATION

1

READS

26

3 AUTHORS:



[Gregorio García](#)

Universidad Politécnica de Madrid

51 PUBLICATIONS 194 CITATIONS

[SEE PROFILE](#)



[Mert Atilhan](#)

Qatar University

101 PUBLICATIONS 962 CITATIONS

[SEE PROFILE](#)



[Santiago Aparicio](#)

Universidad de Burgos

120 PUBLICATIONS 1,477 CITATIONS

[SEE PROFILE](#)

Theoretical Study on the Solvation of C₆₀ Fullerene by Ionic Liquids II: DFT Analysis of the Interaction Mechanism

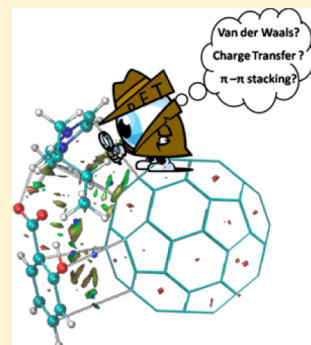
Gregorio García,[†] Mert Atilhan,[‡] and Santiago Aparicio*,[†]

[†]Department of Chemistry, University of Burgos, 09001 Burgos, Spain

[‡]Department of Chemical Engineering, Qatar University, P.O. Box 2713, Doha, Qatar

S Supporting Information

ABSTRACT: As a continuation of our previous work (*J. Phys. Chem. B*, **2014**, *118*, 11330) on the solvation of C₆₀ by ionic liquids (ILs) using Molecular Dynamic simulations, this paper reports a systematic density functional theory (DFT) analysis on the interaction mechanism between C₆₀ and 24 different ionic liquids (belonging to the imidazolium, piperazinium, and cholinium groups). Properties such as binding energies, charge distributions, intermolecular interactions, or electronic structure were analyzed as a function of the selected ILs. The stronger IL-C₆₀ interactions would be related with π–π stacking between the C₆₀ surface and anions such as silylate ([SA]). Likewise, the electronic structure analysis pointed to a well-defined relationship between the energetics of IL-C₆₀ systems and IL features. Therefore, ILs with deep HOMO energies as well as weak interaction between both ions would be a priori good candidates for C₆₀ solvation. Although only short-range interactions are studied in the framework of DFT, this work provides useful information for the rational design of ILs that could exhibit suitable features as C₆₀ solvents.



1. INTRODUCTION

Fullerene C₆₀ is composed of 60 carbon atoms in a hollow sphere arrangement. Since its discovery in 1985 by Smalley et al.,¹ a new area of research has been developed involving fields such as material science, electronics, biomedicine, cosmetics, and fuel cells.² A key step for the successful technological application of fullerenes is their behavior in solution.² Nevertheless, the low water solubility of C₆₀ is well known, whereas aromatic and nonpolar solvents are considered (relatively) good solvents.^{2,3} Therefore, a large collection of studies to improve the solubility of fullerene C₆₀, to hinder its tendency to self-aggregation, have been developed considering solubility data, solution thermodynamics, and several physicochemical properties of fullerenes in solution. The state-of-the-art of this research field has been reviewed by Mchedlov-Petrossyan,² Hua et al.,⁴ and Chaban et al.⁵ The main conclusions of these works are rather pessimistic, with high C₆₀ solubilities being mostly discarded with current approaches and showing the need to develop new methods for fullerene dispersion.

Molecular modeling is a powerful tool for studying C₆₀ solubility as proven by the published work dealing with understanding C₆₀ solvation in several solvents. The majority of these publications are based on the applications of classic Molecular Dynamics (MD) methods.^{4–11} Nevertheless, density functional theory (DFT) simulations¹² or quantitative structure properties relationship (QSPR)¹³ studies have also been published. Among the new alternatives studied for C₆₀ dispersion in solvents, the recent work by Chaban et al.⁵ and Fileti et al.⁸ hypothesized, using computational chemistry approaches, that the solubility of C₆₀ in room temperature ionic

liquids (ILs), based on imidazolium cation and tetrafluoroborate anion, is higher than those previously reported in other traditional solvents,⁵ thus opening a new way for C₆₀ solubilization.

ILs show unique properties, including good thermal and chemical stability, nonflammability, and almost null vapor pressure. All these features have been proven to be useful for many applications in fields such as energy, lubrication, catalysis, synthesis, gas separation, or pharmaceutical applications.¹⁴ Nevertheless, the major advantage of ILs is the possibility to design task-specific solvents through suitable ion combinations, which requires a deep understanding of structure–property relationships.^{14–17} The large number of ILs (~10⁶ only considering pure ILs) leads to the need for systematic approaches for studying the ability of ILs for the considered applications to obtain the most suitable fluid. Unfortunately, this large number of ILs hinders systematic experimental studies, because of economical and temporal constraints, and thus, this is a typical research context in which molecular modeling can provide valuable information for developing new materials in a bottom-up approach and for guiding experimental studies. Therefore, based on the previous relevant initial results for the solvation and dispersion of fullerenes using ILs,^{5,8} we have recently reported a study on C₆₀ solvation in 24 different ILs (containing imidazolium, cholinium, and piperazinium cations paired with eight different types of anions; Figure 1) through MD methods.⁷ One of the main conclusions of this

Received: April 15, 2015

Revised: July 23, 2015

Published: July 24, 2015

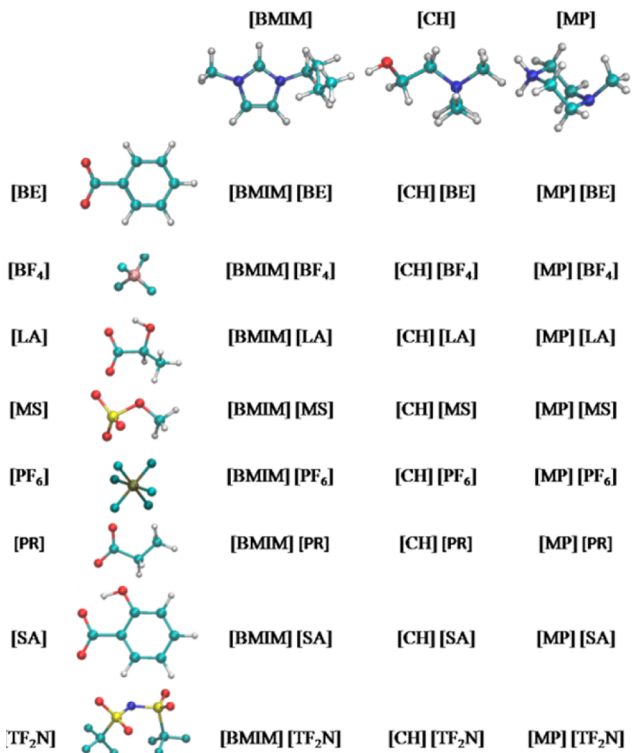


Figure 1. Molecular structure of different ions considered in this work.

work was that the solvation shells around the C_{60} shell are characterized by a strong tendency to develop anion/cation– C_{60} π – π interactions, i.e., those ions with aromatic units would bring out strong ion– C_{60} interactions hindering fullerenes' self-aggregation.

Although only short-range interactions are considered in DFT simulations and systems with large numbers of atoms cannot be studied with a reasonable computational time, DFT could provide useful information at the molecular level on the key parameters related with C_{60} solvation: e.g., ion– C_{60} interaction energies as well as IL– C_{60} charge transfer (CT). Likewise, DFT simulations could also provide the required information for the force field parametrization used for MD. In our previous work, the force field used for MD simulations was refined to reproduce the properties of IL– C_{60} complexes calculated from DFT simulations.⁷ To the best of our knowledge, the only work dealing with DFT calculations to study C_{60} solvation was published by Jang et al.¹² Although this work is focused on C_{60} –water interactions, it revealed important information at the molecular level on C_{60} solubility in water: negative fullerene surface potential along hydrogen bonding network around C_{60} is the main driving force for C_{60} self-aggregation in water.

As a continuation of our previous work,⁷ a detailed DFT analysis on the interaction mechanism between C_{60} and ILs (see Figure 1) is reported in this work. Systems formed by one ionic pair paired with one C_{60} molecule were optimized, for which binding energies, interaction mechanism, charge transfer, and electronic structure were analyzed. The main objective of this work is obtaining a deep understanding of IL solvent– C_{60} interactions from a molecular point of view, which could provide useful information for the rational design of new solvents based on ILs for C_{60} .

2. COMPUTATIONAL METHODS

Systems composed of one isolated molecule (i.e., isolated ions and C_{60}) up to systems composed of both ions + C_{60} were optimized at the B3LYP-D2/6-31G* theoretical level. The optimized minima were checked through their vibrational frequencies. For those simulations wherein two or more molecules are present, different starting points were employed in order to study different relative dispositions, focusing our attention on the configuration with minimal energy. Initial geometries of IL– C_{60} systems were generated from previously published molecular dynamics simulations.⁷ Thus, a cluster formed by one C_{60} and ions in its first solvation shell (20 ion pairs) was extracted. Then, we selected the closest anion to the C_{60} surface, while the paired cation was selected to keep the main interaction between both ions as reported in section 3.1. The same procedure was done focusing on the closest cation to the C_{60} surface. For each IL– C_{60} system, both geometries were fully optimized. The most stable geometry of each IL– C_{60} was further used for the discussion. B3LYP^{18–20} has been selected since it has shown remarkable performance over a wide range of systems,²¹ while dispersion corrections (D2) are adequate since we are considering systems with dispersive interactions such as hydrogen bonds or π – π interactions.²² Likewise, the calculated energies after dispersion corrections are comparable to more accurate values, such as those obtained at the MP2 level.²³ Hence, single point calculations were also carried out over optimized geometries at the MP2/6-31G* theoretical level for isolated ionic liquids. The energies of ILs and IL– C_{60} systems were corrected through the counterpoise method²⁴ for minimizing the basis set superposition error (BSSE).

There are different methods for calculating atomic charge populations, such as the Mulliken method,²⁵ whose basis set dependence is well-known.²⁶ Charge transfer between C_{60} and IL has been studied in this work using both Hirshfeld²⁷ and ChelpG²⁸ methods. The ChelpG scheme has proven to be suitable for describing atomic charges in ILs,^{29–33} while the Hirshfeld model is an alternative definition of atomic charges based on partitioning of the electron density.²⁷ Intermolecular interactions were characterized through both a topological analysis of the electron density according to Bader's³⁴ theory (atoms in molecules, AIM) and the analysis of the reduced density gradient (RGD) at low densities.³⁵ According to AIM theory,³⁴ there are four kinds of critical points, but given the characteristics of the studied systems and to improve and clarify the data analysis, special attention was paid to bond critical points (BCP), which show the criteria for considering the presence of intermolecular interactions, through the computed electronic density (ρ) and its laplacian ($\nabla^2\rho$). Nevertheless, additional information regarding the adsorption on the C_{60} surface could be inferred from the ring and cage critical points (RCP and CCP, respectively). RGD analysis is able to find noncovalent interactions based on the peaks that appear at low densities. Thus, the visualization of RGD iso-surfaces for these peaks allows the visualization of weak interactions. The strength and the nature of the interactions is quantified through the sign of the second density Hessian eigenvalue.³⁵ All calculations were carried out using the Gaussian 09 package,³⁶ whereas AIM and RGD analysis were carried out using MultiWFN code.³⁷ Total and partial density of states (DOS and PDOS, respectively) were calculated using GaussSum code.³⁸

3. RESULTS

3.1. Ionic Liquids. Selected ILs are based on three different cation types: 1-butyl-3-methylimidazolium ([BMIM]), cholinium ([CH]), and methylpiperazinium ([MP]), paired with benzoate ([BE]), tetrafluoroborate ([BF₄]), lactate ([LA]), methylsulfonate ([MS]), hexafluorophosphonate ([PF₆]), salicylate ([SA]), propanoate ([PR]), and bis(trifluoromethylsulfonyl)imide ([TF₂N]) anions. Figure 2

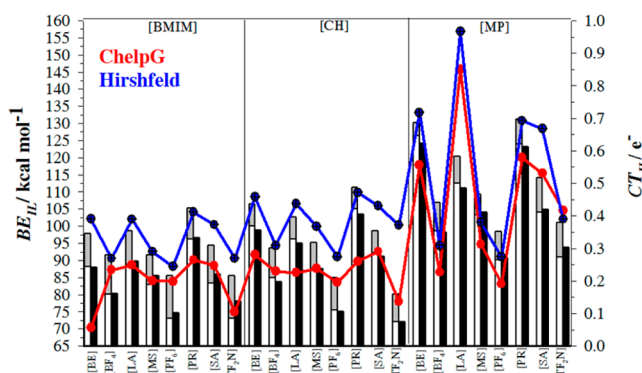


Figure 2. Binding energies for selected ILs (BE_{IL}): white + gray bars, wherein the gray bar stands for dispersion contribution at B3LYP-D2/6-31G*, while black bars stand for values calculated at MP2/6-31G*. Charge transfer (CT_{IL}) computed according ChelpG (red line) and Hirshfeld models (blue line).

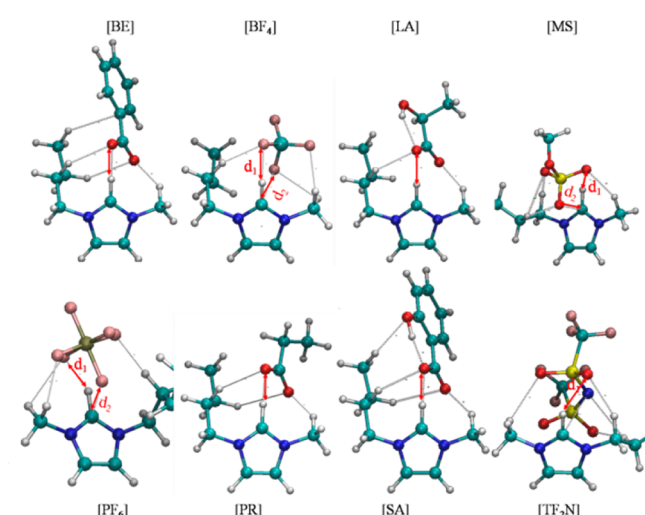


Figure 3. Optimized geometries of [BMIM]-based ILs. Intermolecular interactions are represented as dotted lines, while red lines stand for the main intermolecular interactions analyzed in this work (see Table 1). BCP were omitted for simplicity. Carbon/Hydrogen/Nitrogen/Oxygen/Sulfur/Fluorine/Phosphorus are represented in light blue/white/blue/red/yellow/pink/green.

shows the binding energies of ILs (BE_{IL}), and Figures 3–5 report the most stable geometries for imidazolium, cholinium, and methylpiperazinium-based ILs. BE_{IL} , which can be used for estimating the interaction strength between both ions, has been defined as

$$BE_{IL} = (E_{\text{cat}} + E_{\text{ani}}) - E_{IL}$$

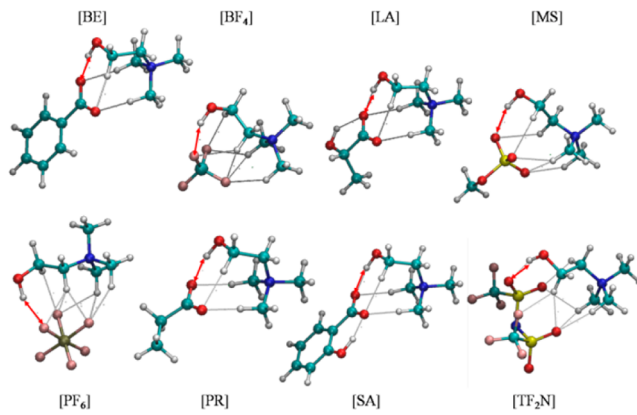


Figure 4. Optimized geometries of [CH]-based ILs. Intermolecular interactions are represented as dotted lines, while red lines stand for the main intermolecular interactions analyzed in this work (see Table 1). BCP were omitted for simplicity. Carbon/Hydrogen/Nitrogen/Oxygen/Sulfur/Fluorine/Phosphorus are represented in light blue/white/blue/red/pink/green.

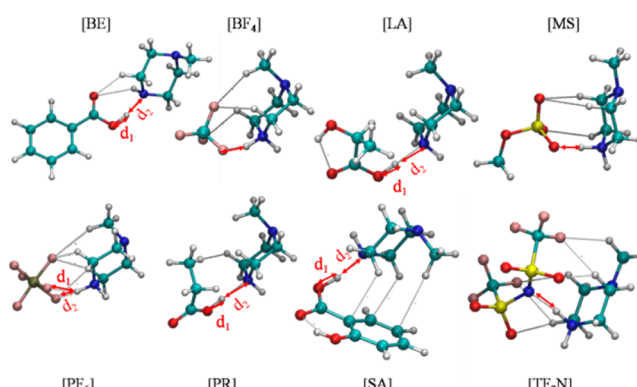


Figure 5. Optimized geometries of [MP]-based ILs. Intermolecular interactions are represented as dotted lines, while red lines stand for the main intermolecular interactions analyzed in this work (see Table 1). BCP were omitted for simplicity.

where E_{cat} , E_{ani} , and E_{IL} stand for the total energy of the cation, anion, and ionic pair, respectively. We have focused on BE_{IL} values estimated at B3LYP-D2/6-31G*. Even though both MP2 and B3LYP-D2 energies follow the same trend, with the dispersion contribution added to B3LYP functional (see below), the main difference between both theoretical levels, i.e., the use of dispersion corrections, is convenient for a proper description of such interactions. Regarding the cation influence (for the same anion), imidazolium and cholinium-based ILs yield similar BE_{IL} , which are smaller than those corresponding to [MP] based ILs. For the anion, the three IL families follow a similar pattern, i.e., $[PR] \geq [BE] \geq [LA] > [SA] > [MS] \geq [BF_4] > [TF_2N] \geq [PF_6]$. The binding energies lie in the range between 131.31 kcal mol⁻¹ ([MP][PR]) and 80.10 kcal mol⁻¹ ([CH][TF₂N]). These high values are mainly due to the important contribution rising from the Coulombic forces between both ions. Figure 2 also displays interionic charge transfers (CT_{IL}) obtained according to ChelpG and Hirshfeld schemes. Although the Hirshfeld populations provide larger CT_{IL} values, both models yield similar trends. As seen in Figure 2, high BE_{IL} values are related to high CT_{IL} . Smaller binding energies for anions such as [BF₄] or [PF₆] would be related with the nature of electronegative atoms. Both anions have 4 or

Table 1. Intermolecular Distances along AIM Parameters Related with Main Intermolecular Interactions (Electronic Density, ρ , and Its Laplacian, $\nabla^2\rho$) between Both Ions of ILs and ILs-C₆₀ 1:1 Complexes

| | IL | | | IL-C ₆₀ | | |
|---------------------------|----------------|--------------|----------------------|--------------------|--------------|----------------------|
| | length /Å | ρ /a.u. | $\nabla^2\rho$ /a.u. | length /Å | ρ /a.u. | $\nabla^2\rho$ /a.u. |
| [BMIM][BE] | 1.725 | 0.0480 | 0.1385 | 2.270 | 0.0176 | 0.0730 |
| [BMIM][BF ₄] | d ₁ | 1.848 | 0.0321 | 0.1083 | | |
| | d ₂ | 2.582 | 0.0186 | 0.0697 | 2.244 | 0.0241 |
| [BMIM][LA] | | 1.763 | 0.0437 | 0.1278 | 1.899 | 0.0343 |
| [BMIM][MS] | d ₁ | 2.406 | 0.0132 | 0.0518 | 1.961 | 0.0289 |
| | d ₂ | 2.922 | 0.0120 | 0.0406 | | |
| [BMIM][PF ₆] | d ₁ | 2.012 | 0.0226 | 0.0837 | 2.083 | 0.0198 |
| | d ₂ | 2.577 | 0.0183 | 0.0703 | 2.584 | 0.0180 |
| [BMIM][PR] | | 1.713 | 0.0498 | 0.1397 | 1.711 | 0.0522 |
| [BMIM][SA] | | 1.778 | 0.0422 | 0.1228 | 2.021 | 0.0262 |
| [BMIM][TF ₂ N] | | 2.281 | 0.0153 | 0.0534 | 2.449 | 0.0110 |
| [CH][BE] | | 1.672 | 0.0502 | 0.1524 | 1.662 | 0.0497 |
| [CH][BF ₄] | | 1.807 | 0.0321 | 0.1072 | 1.826 | 0.0307 |
| [CH][LA] | | 1.688 | 0.0483 | 0.1477 | 1.749 | 0.0402 |
| [CH][MS] | | 1.843 | 0.0327 | 0.1032 | 1.787 | 0.0409 |
| [CH][PF ₆] | | 1.931 | 0.0239 | 0.0811 | 2.033 | 0.0188 |
| [CH][PR] | | 1.660 | 0.0517 | 0.1552 | 1.916 | 0.0415 |
| [CH][SA] | | 1.685 | 0.0484 | 0.1487 | 1.630 | 0.0535 |
| [CH][TF ₂ N] | | 1.845 | 0.0321 | 0.1038 | 1.923 | 0.0266 |
| [MP][BE] | d ₁ | 1.026 | 0.2832 | -1.2957 | 1.024 | 0.3068 |
| | d ₂ | 1.661 | 0.0614 | 0.1317 | 1.786 | 0.0465 |
| [MP][BF ₄] | | 1.597 | 0.0556 | 0.1834 | 1.679 | 0.0487 |
| [MP][LA] | d ₁ | 1.014 | 0.2950 | -1.3945 | 0.999 | 0.2883 |
| | d ₂ | 1.704 | 0.0563 | 0.1282 | 1.735 | 0.0559 |
| [MP][MS] | | 1.526 | 0.0735 | 0.1911 | 2.244 | 0.0169 |
| [MP][PF ₆] | d ₁ | 1.744 | 0.0193 | 0.0780 | 1.706 | 0.0425 |
| | d ₂ | 2.060 | 0.0392 | 0.1300 | 2.110 | 0.0173 |
| [MP][PR] | d ₁ | 1.005 | 0.3053 | -1.4850 | 0.994 | 0.2880 |
| | d ₂ | 1.745 | 0.0515 | 0.1220 | 1.721 | 0.0572 |
| [MP][SA] | d ₁ | 1.018 | 0.2899 | -1.3542 | 1.421 | 0.2328 |
| | d ₂ | 1.701 | 0.0569 | 0.1268 | 1.138 | 0.0077 |
| [MP][TF ₂ N] | | 1.635 | 0.0627 | 0.1487 | 1.681 | 0.0563 |

6 fluorine atoms, i.e., the negative charge is formally delocalized over all fluorine atoms, while in anions such as [PR], [BE], [LA], or [SA] the charge is mainly in the COO⁻ group, which allows a higher charge transfer from the anion to the cation. It is well-known that Coulombic forces between ions play the main role in the interaction between ions. Nonetheless, other intermolecular interactions (such as hydrogen bonding) could also contribute to BE_{IL}. As seen in **Figure 2**, dispersion energy contribution (BE_{dis,IL}, gray region) to the total binding energy (quantified according to Grimme's approach²² for the B3LYP-D2 functional) represents a small component to the total BE_{IL}. Aromatic cations ([BMIM]) yield larger BE_{dis,IL} and high CT_{IL} values are associated with low dispersion contributions.

Intermolecular interactions between both ions were analyzed through AIM theory. In **Figures 3–5**, intermolecular interactions are represented as dotted lines (BCPs were omitted for clarity). In this paper, we have focused on the main interactions (red arrows) between both ions. **Table 1** gathers bond lengths for the main, stronger, intermolecular interactions along the AIM properties of their corresponding BCPs. Atoms involved in these intermolecular interactions (mainly hydrogen bonds) depend on the nature of the ions, i.e., for [BMIM]/[CH]/[MP] based ILs, hydrogen atoms corresponding to -CH group between both N atoms/to OH group/to tetrasubstituted N act

as H bond donors; while COO⁻ groups in anions such as [BE], [LA], [PR], [SA], or, in general, electronegative atoms such O, F, or N play as H bond acceptors. For [MP]-based ILs with a COO⁻ group in the anion ([MP][BE], [MP][LA], [MP][PR], and [MP][SA]) there is a proton transferred from the cation up to the anion. Thus, for [MP][BE], the intermolecular bond between H and the COO⁻ group (d₁) yields a distance of 1.026 Å. Likewise, AIM properties for its associated BCP (high electronic density and negative Laplacian) point out a covalent interaction, whereas d₂ exhibits features of an intermolecular H-bond. Such proton transfer process would lead to higher BE_{dis,IL} (**Figure 2**).

Figure 6 shows BE_{IL} of ILs interacting with the C₆₀ surface (calculated using the IL geometry taken from IL-C₆₀ optimized structures), while bond lengths and AIM properties for the main interactions are reported in **Table 1**. Interactions with the C₆₀ surface promote changes on IL geometries. This new arrangement between ions often leads to an interionic distance elongation, which softens intermolecular interactions as well as reduces Coulombic forces. Concerning imidazolium-based ILs, the most dramatic changes are noted for [BMIM][BE] (14.08 kcal mol⁻¹) and [BMIM][SA] (4.49 kcal mol⁻¹), i.e., ILs with an aromatic anion. These binding energy diminutions can be explained considering the structural rearrangements in ions for

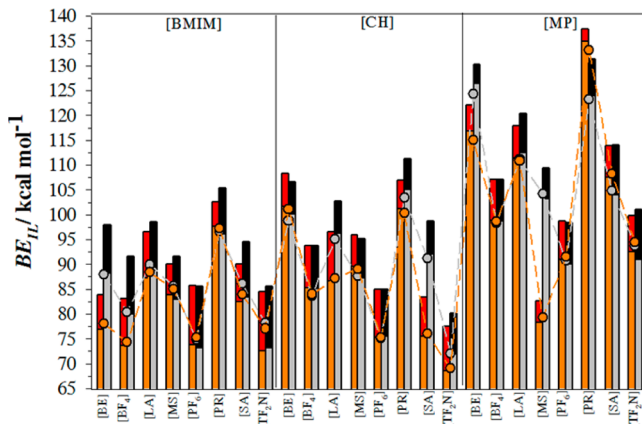


Figure 6. Interionic binding energies between ions (BE_{IL}) of IL- C_60 systems (orange bars) and isolated ILs (gray bars), wherein red and black regions stand for dispersion contributions to the total binding energies. Filled circles represent interionic binding energies computed at the MP2/6-31G* theoretical level.

improving the interactions with C_60 molecule. Therefore, the intermolecular H-bond between both choline and [BE]/[SA] suffers an elongation $\approx 0.545 \text{ \AA}/0.243 \text{ \AA}$ with the consequent electronic density diminution (Table 1). As discussed below, $\pi-\pi$ stacking interactions between C_60 surface and [BE]/[SA] bring on a BE_{IL} decrease.

Regarding the [CH] family, [CH][BE] and [CH][MS] ionic liquids barely increase their BE_{IL} (1.74 kcal mol⁻¹ and 0.88 kcal mol⁻¹, respectively). In both cases, the new arrangement between ions enables new interactions (very weak) between the anion (through the oxygen atoms) and choline cation (through methyl hydrogen atoms), whereas the main H-bond between both ions does not suffer important changes. As seen below, larger decrease on BE_{IL} (15.27 kcal mol⁻¹) for [CH][SA] is due to $\pi-\pi$ stacking between [SA] anion and the fullerene surface. The proton transfer effect described for some piperazine based ILs is also present even in the presence of fullerene molecule, being [MP][PR] the only IL which increases its BE_{IL} .

As previously noted, both B3LYP-D2 and MP2 methods yield similar trends for BE_{IL} , where the main difference between both methods is due to the dispersion corrections added to B3LYP functional.

3.2. Ionic Liquids- C_60 Systems: Binding Energies.

From a molecular viewpoint, IL solvation capability would be related to the strength of the IL- C_60 interactions, i.e., strengthening ion- C_60 interactions is needed for hindering C_60 tendency for self-aggregation. Binding energies for the interaction between selected ILs and C_60 molecule were estimated as

$$BE_{IL-C_60} = (E_{C_60} + E_{IL}) - E_{IL-C_60} \quad (2)$$

where E_{C_60} , E_{IL} , and E_{IL-C_60} are the total energy of fullerene, ionic pair, and IL- C_60 , respectively. As seen from Figure 7, the low values of the binding energies, which range between 7.12 kcal mol⁻¹ ([BMIM][TF₂N]) and 17.08 kcal mol⁻¹ ([BMIM]-[SA]), prove that van der Waals interactions would be the main contribution to the interaction energy. As seen below, this fact agrees with green regions of RGD isosurfaces. Except for [TF₂N] anion, the binding energy values of ILs based on [BMIM] are >3.20 kcal mol⁻¹ than those values estimated for [CH] based ILs. Binding energy values of both choline and imidazol families follow similar order as a function of the anion

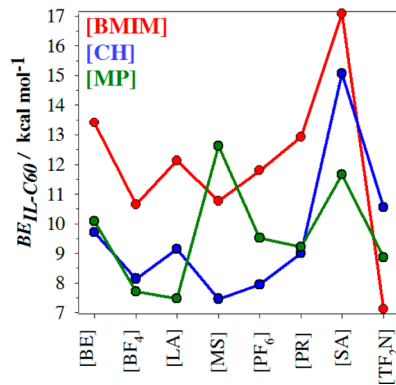


Figure 7. Binding energies for the interaction between ILs and C_60 (BE_{IL-C_60}) computed at the B3LYP-D2/6-31G* level.

([SA] > [BE] > [PR] > [LA] > [PF6] ≥ [BF4] > [MS] > [TF₂N] for imidazolium family). ILs based on piperazinium cation also follow a similar pattern, i.e., larger interaction energies are obtained for [SA] (11.65 kcal mol⁻¹) and [BE] (10.09 kcal mol⁻¹) anions, whereas low values are also related to the [TF₂N] anion (8.86 kcal mol⁻¹). Nevertheless, [MP][MS] provides the strongest interaction with C_60 (8.86 kcal mol⁻¹). Except for this IL, interaction energies of [MP] based ILs with C_60 are, in general, similar to or slightly lower than those predicted for cholinium ones.

The binding energy values indicate that the nature of both cation and anion type, as well as the arrangement between both ions, have important effects on the interaction energies between ILs and fullerene molecule. [MP]-based ILs tend to yield the largest BE_{IL} values, whereas the interaction energies of [MP] based ILs with C_60 molecule lie in the low limit (Figure 7). Thus, the strong interaction between [MP] cation and the selected anion hinders ion- C_60 ones. Regarding the nature of the cation (keeping the anion), imidazolium-based ILs lead to the strongest interactions, mainly due to $\pi-\pi$ stacking interactions between the aromatic imidazolium ring and C_60 surface. Similar conclusions could be extracted from those ILs based on [BE] and [SA] anions.

The literature dealing with the interaction between C_60 and different solvents using DFT is still scarce. According to our knowledge, only Choi et al.¹² published some binding energy values of C_60 -solvent (water in this case) interactions at DFT level (B3LYP/6-31G**). Binding energies reported here are much larger than those estimated for C_60 -water (~ 1.00 kcal mol⁻¹). Moreover, Chaban et al. pointed out the solvation capability of the [BMIM][BF₄] ionic liquid.^{5,6} In this work, $BE_{IL-C_60} = 10.66$ kcal mol⁻¹, which can be considered as a low limit from which larger BE_{IL-C_60} could be a good starting point for the search of new ILs with improved solvation features.

3.3. Ionic Liquids- C_60 Systems: Interaction Mechanism.

Based on interaction energies between ILs and C_60 , there are two key factors that should be needed to consider for maximizing BE_{IL-C_60} values: (i) ILs with low BE_{IL} between both ions and (ii) aromatic ions. This section seeks more information on the main factors governing the interaction mechanism. The charge distribution of IL- C_60 systems was analyzed according to ChelpG (Figure 8) and Hirshfeld (Figure 1S, Supporting Information) models for investigating the role of Coulombic forces. Likewise, the total charge over both ions for isolated ILs is also displayed in Figures 8 and 1S (Supporting Information) for viewing the charge distribution

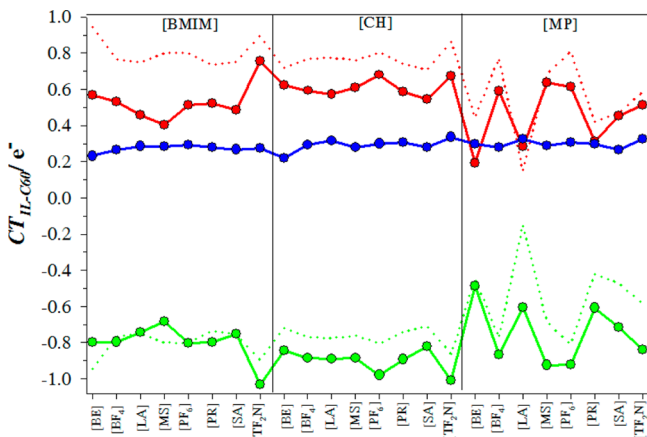


Figure 8. Charge distribution over C_{60} (blue), cation (red), and anion (green) according ChelpG scheme. Dotted lines correspond to ion charges of isolated ILs.

changes over both ions due to the presence of fullerene. ChelpG and Hirshfeld methods provide similar patterns, although charge distribution changes due to C_{60} molecules as well as charge over this molecule are larger according with ChelpG scheme. From now on, the analysis will be centered on ChelpG charges, although similar conclusions could be drawn based on Hirshfeld ones. As seen in Figure 8, the interaction of selected ILs with C_{60} causes the latter to become positively charged by (on average) 0.29 e^- , there is some charge transfer from the fullerene to the cation and anion.

Dispersion forces have been featured through topological analysis of the electronic density (AIM theory) and RGD isosurfaces, Figures 9, 11, and 12. Those figures also show the

intermolecular cation/anion (red/green color) interactions along with their lengths and the corresponding BCP. RGD iso-surfaces are displayed in Figures 10, 2S and 3S (Supporting Information). The visualization of RGD iso-surfaces for the peaks that appear at low densities allows the localization of weak interactions, wherein the strength and nature of the interactions is determined through the sign of the second density Hessian eigenvalue.³⁵ The green color of the regions between the IL and C_{60} molecule points out van der Waals interactions. As expected, there are similarities between CPs found through AIM theory and RGD isosurfaces.

Aimed at studying all BCps as a whole, we have analyzed the total electronic density sum over all BCps ($\sum\rho_{(BCP)}$, black line in Figure 13) related with IL $\cdots C_{60}$ interactions. In addition, based on the atoms involved in each interaction, $\sum\rho_{(BCP)}$ can be defined as the sum of contributions from cation/anion $\cdots C_{60}$ interactions (red/green line in Figure 13): $\sum\rho_{(BCP)} = \sum\rho_{(BCP,cat)} + \sum\rho_{(BCP,ani)}$. The total electronic density over all RCPs and CCPs ($\sum\rho_{(RCP)}$ and $\sum\rho_{(CCP)}$, respectively) associated with IL $\cdots C_{60}$ interactions are also drawn in Figure 15 (blue and orange lines, respectively). Note that $\sum\rho_{(RCP)}$ and $\sum\rho_{(CCP)}$ follow the same trend. Palusiak et al.³⁹ found that the ring critical point features (mainly the electronic density, ρ) should reflect some characteristic properties of the ring (or quasi-ring), e.g., π -electronic delocalization. One of the main conclusions was that the physical meaning of the electron density is connected with the electronic delocalization. On the basis of these previous results, we have hypothesized the connection between electronic delocalization between IL and C_{60} and $\sum\rho_{(RCP)}$ and $\sum\rho_{(CCP)}$ values.

Based on data reported in Figures 7–13, the following paragraphs describe the general trends noted for each IL family

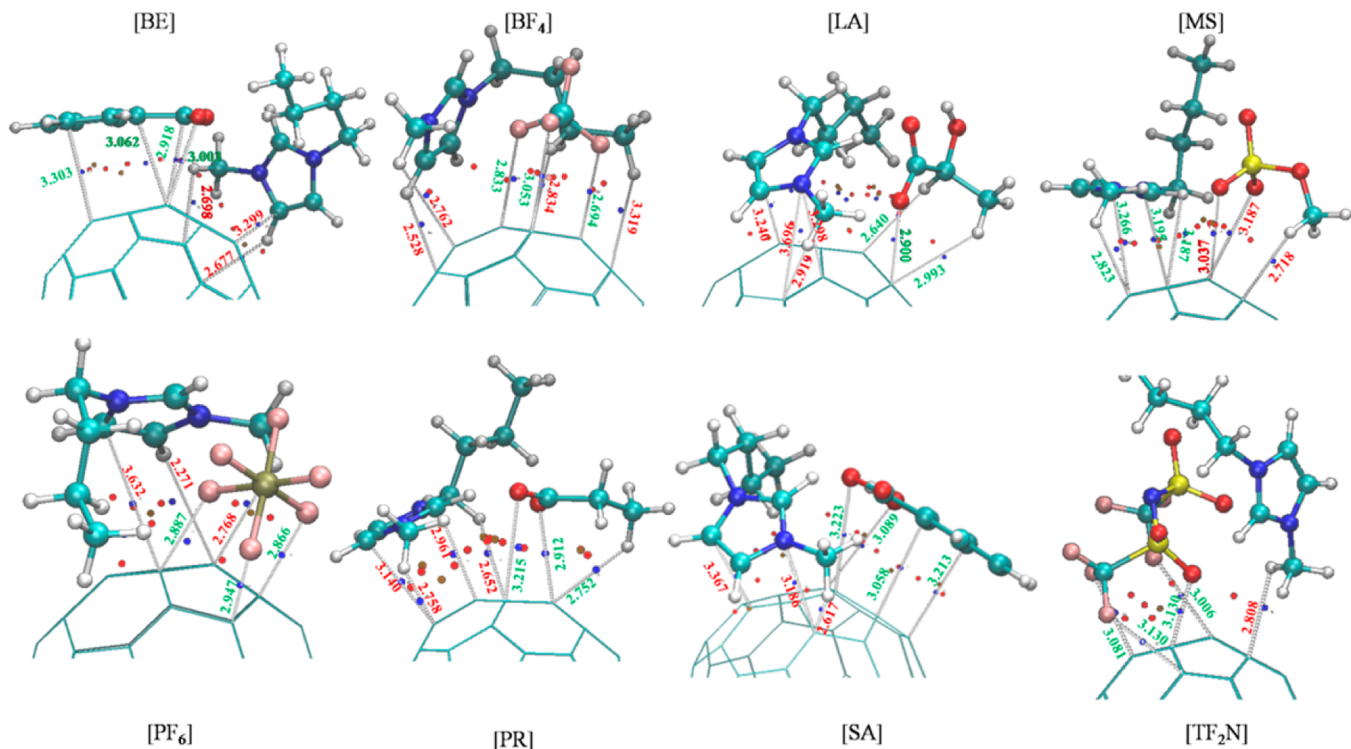


Figure 9. Optimized structure corresponding to IL- C_{60} systems for imidazolium based ILs main intermolecular IL $\cdots C_{60}$ interactions (cation/anion $\cdots C_{60}$ interactions are displayed in red/green color). Intermolecular bond lengths are in angstroms. Blue, red, and purple points stand for BCps, RCPs, and CCPs, respectively, related with intermolecular interactions. For simplicity, intermolecular interactions between ions were omitted.

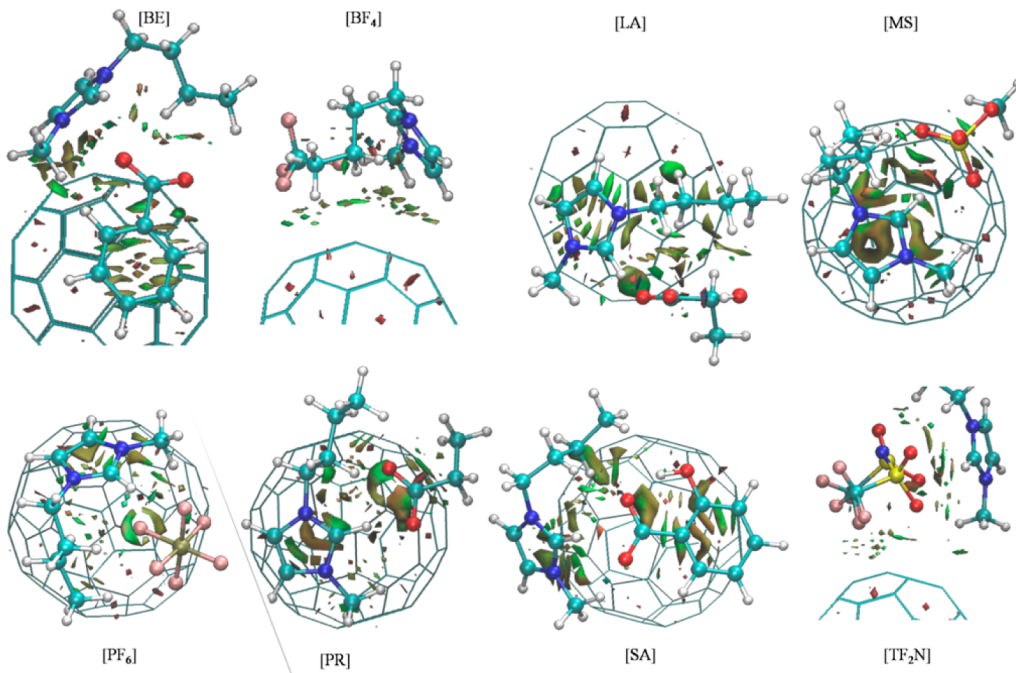


Figure 10. Bottom: RGD iso-surfaces of IL...C₆₀ systems for imidazolium based ILs.

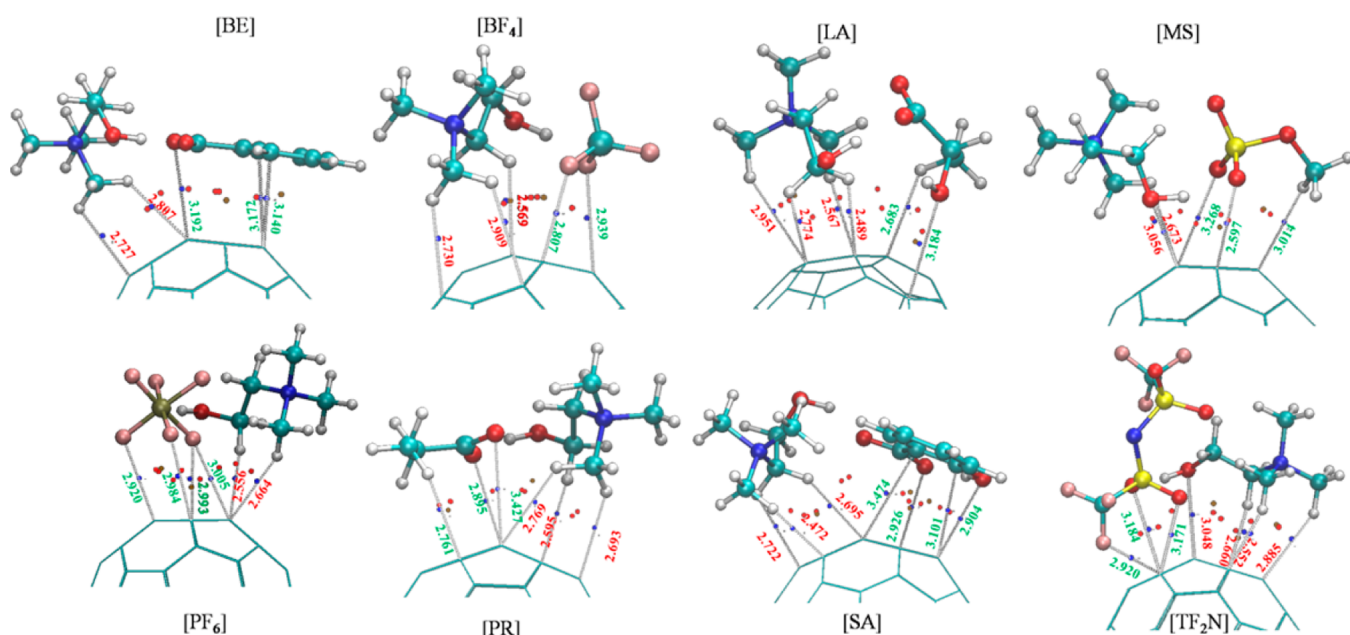


Figure 11. Optimized structure corresponding to IL-C₆₀ systems for cholinium based ILs along main intermolecular IL...C₆₀ interactions (cation/anion...C₆₀ interactions are displayed in red/green color). Intermolecular bond lengths are in angstroms. Blue, red, and purple points stand for BCPs, RCPs, and CCPs, respectively, related to intermolecular interactions. For simplicity, intermolecular interactions between ions were omitted.

(i.e., imidazolium, choline, and piperazine-based ILs) as well as the main differences between ILs from the same family. To analyze possible relationships between binding energy, charge transfer, and dispersion forces (assessed thorough AIM), BE_{IL-C₆₀} and C₆₀ charge are also included in Figure 13 (pink and gray dotted lines, respectively).

3.3.1. Imidazolium-Based Ionic Liquids. The order for BE_{IL-C₆₀} values is [SA] > [BE] > [PR] ≥ [LA] > [PF₆] > [MS] ≈ [BF₄] > [TF₂N], with the weakest IL...C₆₀ interactions for [BMIM][TF₂N], [BMIM][BF₄], and [BMIM][PF₆]. Likewise, all those anions with F atoms show some similarities in the

interaction mechanism. In the absence of C₆₀ molecule, BE_{IL} values of [BMIM][BF₄]/[BMIM]/[PF₆]/[BMIM][TF₂N] are mainly due to an interionic CT = 0.23 e⁻/0.20 e⁻/0.10 e⁻, although BE_{dis,IL} (11.54 kcal mol⁻¹/12.48 kcal mol⁻¹/12.42 kcal mol⁻¹) offer an important contribution (see Figure 2). Due to the interactions with fullerene molecules, BE_{IL} values are not importantly affected for [BMIM][PF₆] and [BMIM][TF₂N], while it decreases 8.46 kcal mol⁻¹ for [BMIM][TF₂N]. BE_{dis,IL} and AIM parameters for interionic interactions are only slightly affected by C₆₀ molecule (see Figure 6 and Table 1). Therefore, BE_{IL} diminution is mainly due to an interionic CT decrease. In

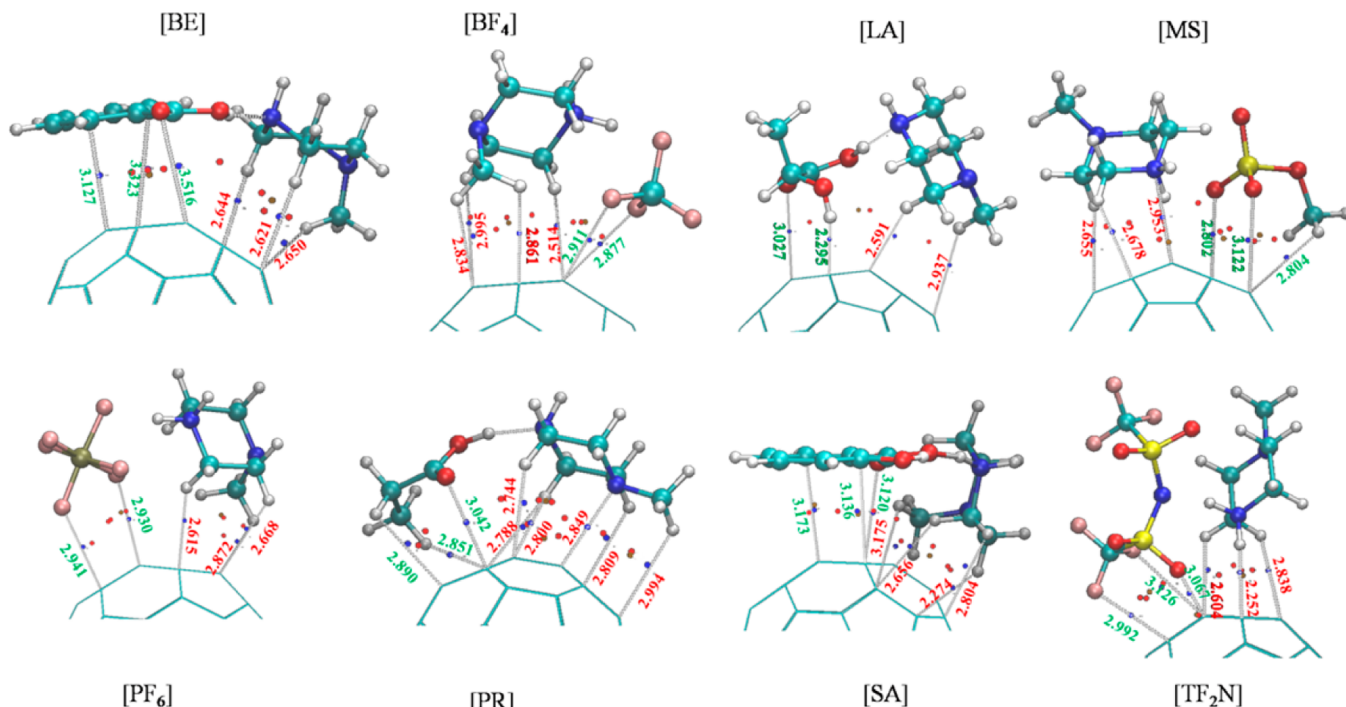


Figure 12. Optimized structure corresponding to IL-C₆₀ systems for piperazinium based ILs along the main intermolecular IL···C₆₀ interactions (cation/anion···C₆₀ interactions are displayed in red/green color). Intermolecular bond lengths are in angstroms. Blue, red, and brown points stand for those BCPs, RCPs, and CCPs, respectively, related with intermolecular interaction. For simplicity, intermolecular interactions between ions were omitted.

fact, [BMIM]⁺ cation becomes less positive, whereas the anions keep their negative charge unaffected (or slightly affected), which induces a positive charge of $\approx 0.28\text{ e}^-$ on the C₆₀ surface, i.e., CT occurs from C₆₀ to the imidazolium cation. There are also some H-bonds between the cation and the surface. However, since most H are alkylic, those H-bonds are very weak, while there are several van der Waals interactions between the C₆₀ surface and fluorine atoms, which are stronger than cation···C₆₀ ones ($\sum\rho_{(\text{BCP},\text{cat})} < \sum\rho_{(\text{BCP},\text{ani})}$). These three ILs yield similar $\sum\rho_{(\text{BCP},\text{ani})}$ values, while the order of $\sum\rho_{(\text{BCP},\text{cat})}$ and $\sum\rho_{(\text{RCP})}$ contributions determines their relative BE_{IL-C₆₀}. Thus, [BMIM][TF₂N] resulted in the weakening of IL···C₆₀ interactions because of the lowest contributions from $\sum\rho_{(\text{BCP},\text{cat})}$ and $\sum\rho_{(\text{RCP})}$. [BMIM][PF₆] allows a π - π stacking interaction with C₆₀ surface (Figure 10), which agrees with increasing $\sum\rho_{(\text{BCP},\text{cat})}$ and BE_{IL-C₆₀}. Therefore, the interaction mechanism is mainly governed by anion···C₆₀ interactions, while the low contributions from cation···C₆₀ interactions hinders more stable IL-C₆₀ systems.

Both [BMIM][BF₄] and [BMIM][MS] yield BE_{IL-C₆₀} $\approx 10.71\text{ kcal mol}^{-1}$. For the latter, similar features are also noted concerning BE_{IL} or charge over fullerene molecule, although some charge transfer from the anion to C₆₀ ([MS] becomes less negative (Figure 8). For this IL, larger O (anion)-C₆₀ lengths lead to lower contribution from $\sum\rho_{(\text{BCP},\text{ani})}$. This lower [MS]-C₆₀ affinity allows a π - π stacking interaction between imidazolium cation and the C₆₀ surface, which agrees with increasing $\sum\rho_{(\text{BCP},\text{cat})}$ and $\sum\rho_{(\text{RCP})}$.

[BMIM][PR] and [BMIM][LA] yield BE_{IL-C₆₀} $\approx 12.53\text{ kcal mol}^{-1}$. Again, there is a CT $\approx 0.28\text{ e}^-$ from C₆₀ to [BMIM] cation (anion charge does not change, Figure 8). AIM parameters are also similar for both compounds. However, there are some differences in the atoms through which anion···

C₆₀ interactions are carried out. Both O atoms (in COO⁻ group) of the [PR] anion are parallel to the C₆₀ surface with length $\approx 3.0\text{ \AA}$. Hence, COO⁻ establishes van der Waals interaction with fullerene molecule (Figures 9 and 10). However, the presence of an OH group in [LA] brings about the formation of an intermolecular H-bond through COO⁻ and OH groups. This intramolecular H-bond develops a *quasi*-ring, which is perpendicular to the C₆₀ surface. In this new arrangement, only O atoms not implicated in intramolecular bonding are able to interact with the C₆₀ molecule. Nonetheless, lower O-C₆₀ length (2.640 Å) permits similar strength compared to [MS]···C₆₀. Despite the presence of intra-molecular H-bonds, both ILs display similar interaction mechanism-related features.

Imidazolium-based ILs with aromatic anions ([BE] and [SA]) leads to strong interactions with the C₆₀ surface in comparison with other imidazolium-based ILs. Both [BMIM]-[BE] (13.41 kcal mol⁻¹) and [BMIM][SA] (17.08 kcal mol⁻¹) provide the largest BE_{IL-C₆₀} within this family. In addition, [BMIM][SA] presents the largest interaction with C₆₀ among all the studied ILs, whereas BE_{IL-C₆₀} of [BMIM][BE] are only surpassed by [CH][SA] and [BMIM][SA] (Figure 7). The [BE] anion tends to be arranged in parallel orientation to the C₆₀ surface (with the distance between both planes $\approx 3.07\text{ \AA}$), which would allow π - π stacking interactions. As a consequence, this IL provides larger $\sum\rho_{(\text{RCP})}$. On the other hand, the [BMIM] cation interacts with C₆₀ via its methyl group and both C and H in position 4. There is some π -stacking between the C=C bond on the C₆₀ surface (distance $\approx 3.30\text{ \AA}$). As seen from Figures 9, 10, and 13, anion-C₆₀ configuration brings out stronger interactions ($\sum\rho_{(\text{BCP},\text{ani})} > \sum\rho_{(\text{BCP},\text{cat})}$). As a consequence of both CT processes (i.e., from [BE] to [BMIM] and from [BMIM] to fullerene molecule)

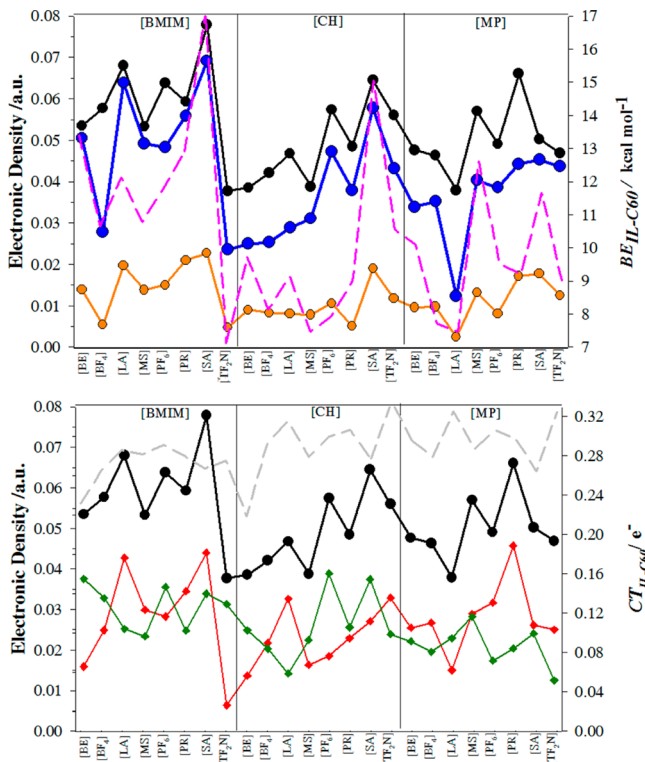


Figure 13. Top: Total sum of electronic density, ρ , for those BCPs, RCPs, and CCPs (black, blue, and orange, respectively) estimated for IL...C₆₀ interactions. Bottom: cation/anion...C₆₀ contributions (green/red) to the total BCP electronic density. Binding energies of IL-C₆₀ interactions (pink dotted line) as well as total charge over fullerene molecule according ChelpG scheme (gray dotted line) are also displayed. Data for this figure are in Table 1S (Supporting Information).

both ions decrease their respective charges in comparison with isolated IL. Concerning [BMIM][SA] ionic liquid, both ions set up π - π stacking with fullerene molecules (see Figure 10). For the [BMIM] cation, this π - π stacking is more efficient than [BMIM][SA]. Although [SA] is also parallel to the C₆₀ surface, π - π stacking is carried out between the C₆₀ surface and the quasi-ring through the intramolecular H-bond between COO⁻ and OH (in ortho position) groups. This new arrangement between both ions over C₆₀ allows a more efficient interaction between both ions (Figure 6), which also permits the presence of new RCPs. As a result, both ionic liquids present similar $\sum\rho_{(BCP,ani)}$ to the total $\sum\rho_{(BCP)}$, whereas larger contributions are obtained from $\sum\rho_{(BCP,cat)}$ and $\sum\rho_{(RCP)}$. Hence, [BMIM][SA] leads to the strongest interaction with the fullerene surface. In addition, CT of [BMIM][SA]-C₆₀ only takes place from the cation up to C₆₀ molecule.

Based on the description of imidazolium family above, it seems that π - π stacking between ions and the fullerene surface would allow efficient ion-C₆₀ interactions. There is also an increasing electronic delocalization between the IL and C₆₀ molecule (high $\sum\rho_{(RCP)}$), which should be an adequate IL feature to hinder C₆₀ aggregation.

3.3.2. Cholinium-Based Ionic Liquids. The ordering for BE_{IL-C₆₀} as a function of the anion is very similar than those described for imidazolium-based ILs, i.e., the largest/lowest values are obtained for aromatic ([BE] and [SA])/[TF₂N] anions. Binding energies of IL-C₆₀ for cholinium based ILs are, in general, of roughly 3.15 kcal mol⁻¹ lower than those ones of

ILs based on [BMIM]. This trend is not found for [CH][TF₂N] (BE_{IL-C₆₀} = 10.56 kcal mol⁻¹) ionic liquids, whose BE_{IL-C₆₀} is 3.45 kcal mol⁻¹ larger than the BE_{IL-C₆₀} of [BE][TF₂N]. Other similar features between both [BMIM] and [CH]-based ILs are also found. For example, larger BE_{IL-C₆₀} values of [CH][BE] and [CH][SA] are mainly due to π - π stacking interactions between C₆₀ and aromatic anions. As said, a stronger π -stacking interaction between [SA] anion and the fullerene surface leads to an important decrease on BE_{IL} of [CH][SA]. In accordance with this large interaction, larger $\sum\rho_{(BCP,ani)}$ values are obtained for [SA] ions in comparison to [BE] (see Figure 13 down).

According to Figure 8, both ions gain negative charge due to interactions with C₆₀. The sign of the charges on the fullerene molecule (on average, 0.29 e⁻) points out that CT is done from C₆₀ to both ions (0.16 e⁻ and 0.13e⁻ to cation and anion, respectively).

[CH]...fullerene interactions depend on the selected ionic liquid. For choline-based ionic liquids, cation-C₆₀ intermolecular bonds are mainly H-bonds between several methyl H atoms and the C₆₀ surface. Hence, they are extremely weak. The presence of intermolecular H-bonds between the C₆₀ surface and -CH₂ adjacent to the OH motif ([CH][BF₄], [CH][MS], [CH][PF₆], [CH][PR]) as well as between O atom and the C₆₀ surface ([CH][MS]) tend to strengthen cation...C₆₀ links. [BMIM][BF₄] and [BMIM][MS] displayed similar features for [BMIM]...C₆₀ interactions or BE_{IL-C₆₀}. Only slight differences between anion...C₆₀ interactions were noted, which are also present in [CH][BF₄] and [CH][MS] ionic liquids. Nonetheless, [CH][MS] ionic liquid yielded lower BE_{IL-C₆₀} than [CH][BF₄]. Lower [CH]...fullerene interactions for [CH][MS] would be mainly due to larger (hence weaker) cation-C₆₀ lengths.

There are several similarities between imidazolium and cholinium-based ionic liquids as an anion function. [CH][LA] and [CH][TF₂N] are the only ones which follow slight different patterns than those reported above for the imidazolium family. Regarding the [CH][LA] ionic liquid, [LA]...C₆₀ interactions are set up between OH group and the C₆₀ surface, while COO⁻ groups do not play any role (Figures 11 and 2S). For the [CH][LA] ionic liquid, based on $\sum\rho_{(BCP,ani)}$ values (Figure 13), the OH...C₆₀ interaction ([CH][LA]) seems to be weaker than the COO⁻...C₆₀ interaction ([BMIM][LA]). Concerning [CH][TF₂N], larger interaction energies are present with C₆₀ than with the homologue with imidazol. Although there are some differences in $\sum\rho_{(BCP,ani)}$ values, the [CH] cation is able to form several intermolecular bonds with the C₆₀ surface, which contribute to larger contributions from cation...C₆₀ interactions to the total IL-C₆₀ binding energy, which are larger than [BMIM][TF₂N]. Similar cation...C₆₀ interactions were noted for [CH][LA]. Unfortunately, less favorable anion...C₆₀ links hinder interaction energies over [BMIM][LA]-C₆₀ systems.

In short, both [BMIM] and [CH]-based ILs yielded similar trends for anion function; although interaction energies of choline-based ionic liquids were lower. However, only a difference of roughly 2.00 kcal mol⁻¹ is obtained for [SA]-based ionic liquids. In addition, choline-based ionic liquids are a new family of ionic liquids with suitable properties such as null toxicity, high biodegradability, or low cost.⁴⁰ Therefore, [CH][SA] could be suggested as an adequate candidate to carry out experimental studies on C₆₀ solvation.

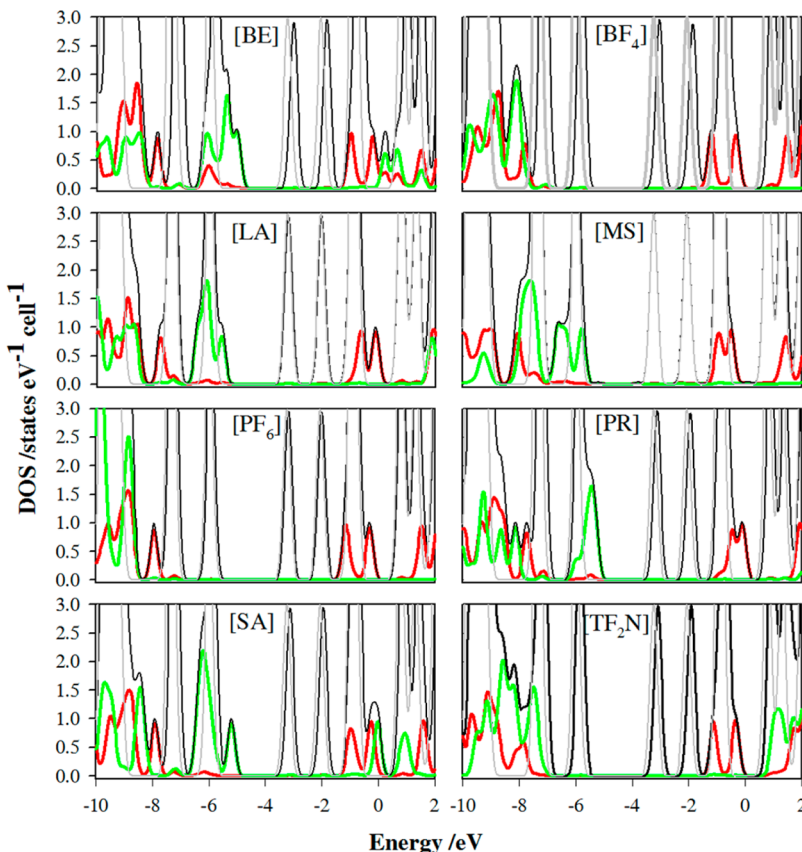


Figure 14. Density of states of IL-C₆₀ for imidazol-based ILs (black), partial density of states (PDOS) of the cation (red) and anion (green), and density of states of pristine C₆₀ (gray).

3.3.3. Piperazinium-Based Ionic Liquids. The binding energy values for IL-C₆₀ systems of ionic liquids based on [MP] follow the order [MS] (12.62 kcal mol⁻¹) > [SA] (11.66 kcal mol⁻¹) > [BE] (10.09 kcal mol⁻¹) > [PF₆] (9.52 kcal mol⁻¹) ≥ [PR] (9.21 kcal mol⁻¹) ≈ [TF₂N] (8.87 kcal mol⁻¹) > [BF₄] (7.72 kcal mol⁻¹) ≥ [LA] (7.48 kcal mol⁻¹). Both ions becomes more negative in the presence of the C₆₀ molecule, for which the total charge is (on average) 0.30 e⁻, which means that there are CT processes from the C₆₀ up to both ions. These CT processes are larger for [MP][BE] and [MP][PR] ionic liquids. However, their BE_{IL-C₆₀} values lie in the low range (see Figure 7). As said, BE_{IL-C₆₀} values agree with interactions through van der Waals interactions, and CT processes would not play an important role.

Ionic liquids such as [MP][BE], [MP][BF₄], [MP][PR], [MP][SA], or [MP][TF₂N] yield BE_{IL-C₆₀} with similar trends in anion function than the other ionic liquid families. Although BE_{IL-C₆₀} of [BMIM][MS] and [CH][MS] lie close to the low limit for each family, interaction energies of [MP][MS]-C₆₀ are the highest within the piperazine-based ILs, even larger than [MP][BE] or [MP][SA]. [MP][MS] displays some characteristics that allow strong interactions with the C₆₀ surface. For example, interactions with C₆₀ molecule reveal that BE_{IL} diminishes from 109.32 kcal mol⁻¹ up to 82.65 kcal mol⁻¹, which represents the largest change. As can be seen in Figure 8, CT from C₆₀ to the [MS] anion causes it becomes more negative, while the [MP] charge remains unchanged. This results in an interionic CT diminution, which agrees with decreasing BE_{IL}. Lower interionic interactions allow improvement of both ion-C₆₀ interactions. As can be seen in Figures

12 and 3S (Supporting Information), [MP]-C₆₀ interactions are mainly carried out through CH₂ ring groups and the C₆₀ surface, whereas O-C₆₀ intermolecular bonds are the main contributor to $\sum \rho_{(BCP,ani)}$. The presence of several intermolecular ion-C₆₀ bonds as well as H-bonding between both ions (d_1 in Figure 5) allows the presence of several RCPs (and CCPs). Likewise, high $\sum \rho_{(RCP)}$ (electronic delocalization between IL and C₆₀) would also contribute to strengthening [MP][MS]...C₆₀ interactions.

Although there are some H-bonds between -CH₂ motifs (piperazine) and the C₆₀, the parallel configuration between [BE] and [SA] anions and the C₆₀ surface allows strong $\pi-\pi$ stacking anion...C₆₀ interactions (see Figures 12, 13, and 3S (Supporting Information)), even if both [BE] and [SA] anions provide similar $\sum \rho_{(BCP,ani)}$. Cation arrangement on C₆₀ of [MP][SA] leads to somewhat larger $\sum \rho_{(BCP,cat)}$ and $\sum \rho_{(RCP)}$ contributions. BE_{IL-C₆₀} values of both ILs are not as high as those of [BMIM][SA] or [CH][BE], though they are close to those of [BMIM][BF₄] ILs. In addition, the piperazine cation also displays adequate properties as a green solvent such as low toxicity, high biodegradability, or low cost,⁴¹ which could allow the use of both ILs as C₆₀ solvents.

The remaining piperazinium-based ILs have led to BE_{IL-C₆₀} values in the low range, which are also lower than BE_{IL-C₆₀} of [BMIM][BF₄]. Thus, based on their interaction energies, these ILs would display inferior properties as possible C₆₀ solvents. As previously described, anion...C₆₀ interactions for those anions with F atoms are carried out through F-C₆₀ surface intermolecular bonds, which contribute to $\sum \rho_{(BCP,ani)} > \sum \rho_{(BCP,cat)}$. For [MP][PR], one oxygen atom (which is not

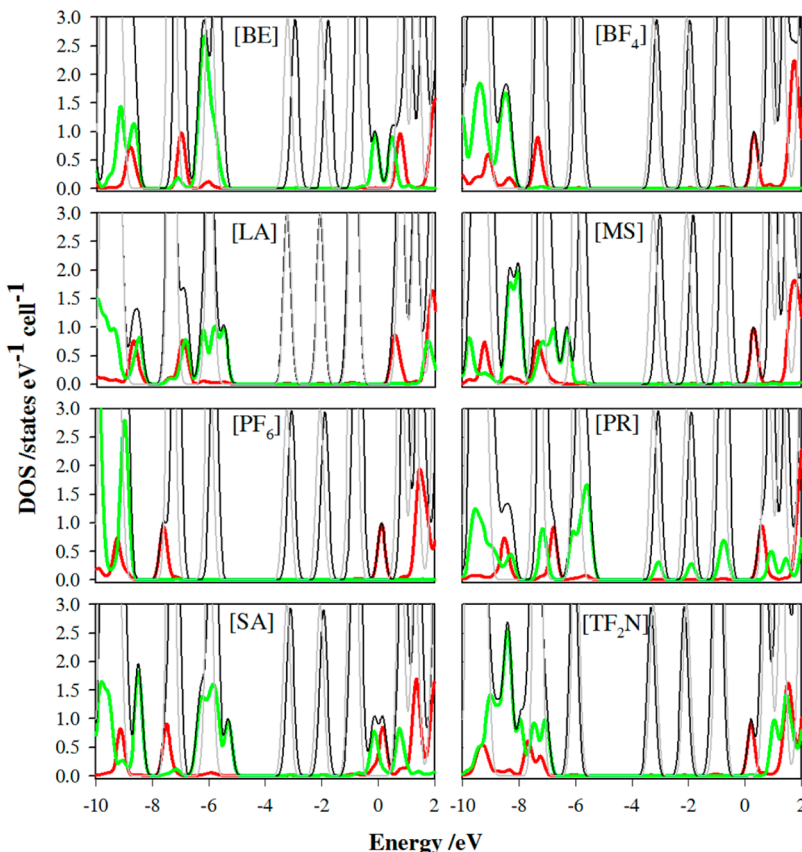


Figure 15. Density of states of IL-C₆₀ for choline based ILs (black), partial density of states (PDOS) of the cation (red) and anion (green), and density of states of pristine C₆₀ (gray).

involved in proton transfer) can establish an intermolecular bond with the C₆₀ surface. As seen in Figure 3S (*Supporting Information*), the isosurface between the carboxylate group and C₆₀ is extended over the entire COO-motif. However, for the [LA] anion, this O atom is adjacent to the OH group, hindering the possibility of an intramolecular H-bond. This behavior permits a new H-bond between the hydroxyl group and the C₆₀ surface; however, other contributions such as $\sum \rho_{(\text{BCP,cat})}$ and $\sum \rho_{(\text{RCP})}$ are very low. As a consequence, [MP][PR]...C₆₀ interaction energies lie in the low range, as small as those of [BMIM]TF₂N] or [CH][MS].

3.4. Ionic Liquids-C₆₀ systems: Electronic Structure.

The analysis of electronic structure could also shed light on the IL-C₆₀ interaction mechanism. Figures 4S (*Supporting Information*) and 14–16 show the density of states (DOS) of the isolated C₆₀ molecule and IL-C₆₀ systems. Even though it is well-known that common GGA functionals are not adequate for predicting accurate orbital energies, this section only pursues the changes on the electronic structure due to the interactions with C₆₀ and the tendency followed as a function of the selected family. Therefore, the electronic structure analysis was also carried out at the B3LYP-D2/6-31G* level. Partial densities of states from both ions are also reported in Figures 14–16. Pristine C₆₀ yields HOMO and LUMO energies equal to -6.04 eV and -3.31 eV, which leads to a HOMO-LUMO energy gap $\Delta E_{\text{H-G}} = 2.73$ eV. The interactions with selected ILs do not have large effects on the fullerene electronic structure, with both HOMO/LUMO levels slightly shifting their energies. Diminution of LUMO energy levels lies between 0.00 and 0.20 eV. The contributions from PDOS of both ions are

characteristic of the selected anion. Thus, cationic PDOS of imidazol-based ionic liquids do not affect the C₆₀ electronic structure, since the major contributions in the vicinity of the C₆₀ HOMO-LUMO gap are two peaks of around -0.06 eV (unoccupied orbitals), while the contributions from the higher occupied orbital over the cation motif appear to be approximately -6.00 eV. Regarding the anion, contributions from the unoccupied orbital to the DOS are far from the LUMO energy of C₆₀. Nonetheless, for some IL-C₆₀ systems, the highest occupied orbital comes from PDOS of the IL motif. Figure 5S (*Supporting Information*) displays the energies corresponding to the highest/lowest occupied/unoccupied orbitals over the ionic liquid (i.e., HOMO and LUMO over ionic liquid motif: HOMO_{IL} and LUMO_{IL}) as well as their $\Delta E_{\text{H-G}}$. These energies are only scarcely affected due to interactions with the C₆₀ surface. In general, aromatic cations provide the lowest LUMO energies (~ -1.0 eV), while LUMO energies are close to zero for [CH] and [MP] ILs. HOMO energies of [BMIM] and [CH]-based ILs are largely affected by the nature of the anion. Three ionic liquid families follow the same patterns and anionic nature, i.e., [BF₄], [PF₆], and [Tf₂N] provide the deepest HOMO energies. Concerning $\Delta E_{\text{H-G}}$, imidazolium and cholinium ILs yield the same evolution as anion function, with $\Delta E_{\text{H-G}}$ of cholinium ILs being larger. Except for [MP][BE] and [MP][SA], $\Delta E_{\text{H-G}}$ of methylpiperazinium-based ILs is vaguely affected by the anion.

LUMO_{IL} energies are far from the LUMO level of C₆₀, while some IL-C₆₀ yield smaller $\Delta E_{\text{H-G}}$ than pristine C₆₀ since HOMO_{IL} energies are somewhat stabilized upon interaction with the C₆₀ surface. These HOMO_{IL} energies could be useful

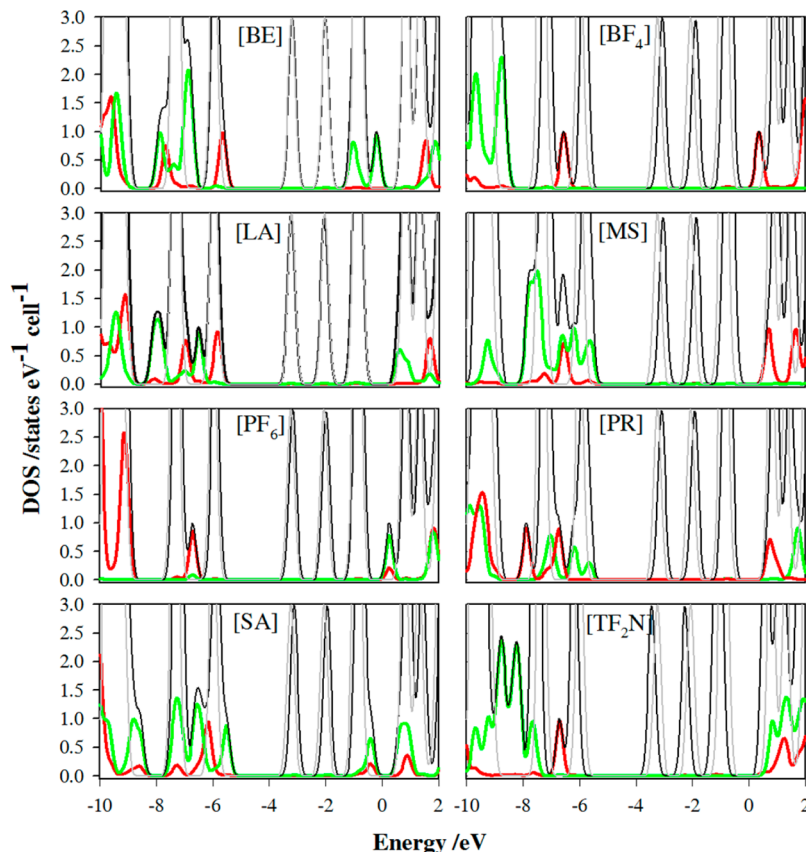


Figure 16. Density of states of IL-C₆₀ for piperazine based ILs (black), partial density of states (PDOS) of the cation (red) and anion (green), and density of states of pristine C₆₀ (gray).

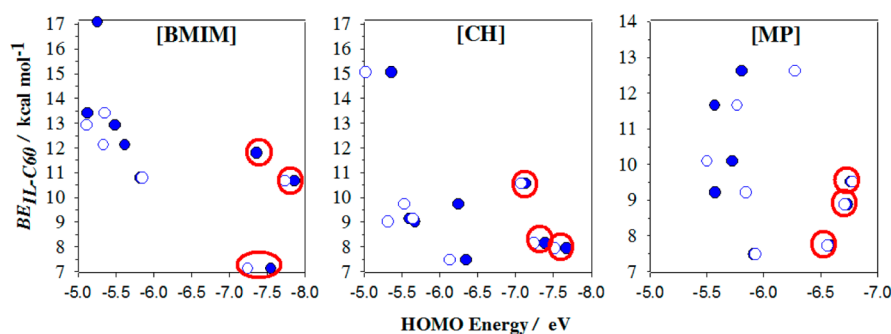


Figure 17. Evolution of BE_{IL-C₆₀} as a function of HOMO_{IL}/HOMO of isolated ILs (filled points/empty points).

for rationalizing the IL-C₆₀ binding energies. [BMIM][SA], [BMIM][BE], [BMIM][PR], [BMIM][LA], and [BMIM][MS] provided the largest IL-C₆₀ binding energies of the imidazol family, and for these ILs, HOMO_{IL} (which mainly comes from PDOS of the anions, Figure 14) energies are higher than HOMO energy of C₆₀, whereas the remaining imidazol-based ILs, which give away lower BE_{IL-C₆₀}, the HOMO_{IL} is mainly located over the cation (except for TF₂N anion) and their energies are deeper than HOMO of C₆₀. Similar conclusions can also be obtained for choline and piperazine-based ILs. For example, HOMO_{IL} of [CH][SA]-C₆₀ and [MP][SA]-C₆₀ are more stable than fullerene HOMO energy, and both ionic liquids lead to high BE_{IL-C₆₀} values. The relationship between HOMO_{IL} (whose energy values are very similar than those obtained for isolated ionic liquids) and BE_{IL-C₆₀} was confirmed with results reported in Figure 17. Therefore, large BE_{IL-C₆₀} values stand on deep HOMO energies for the isolated ILs. In

addition, these HOMO orbitals should be mainly localized on the anion. These connections between BE_{IL-C₆₀} and HOMO energies are not followed by ILs with fluorine atoms in the anions ([BF₄], [PF₆], and [TF₂N]). These ILs not only provide low HOMO, but their HOMO_{IL} are over the cation. Likewise, the interionic biding energies of ILs based on [BF₄], [PF₆], and [TF₂N] (Figure 2) are in the lower limit in comparison with other ILs within the same family. Therefore, not only deep HOMO energies (mainly located over the anion), but also low BE_{IL} for the isolated ionic pairs are need to improve IL-C₆₀ interactions.

4. CONCLUSIONS

A systematic analysis of the interaction mechanism between the fullerene C₆₀ molecule and three types of ionic liquids (ILs) based on imidazol ([BMIM]), choline ([CH]), and piperazine

([MP]) cations along with anions such as benzoate ([BE]), tetrafluoroborate ([BF₄]), lactate ([LA]), methylsulfonate ([MS]), hexafluorophosphonate ([PF₆]), salicylate ([SA]), propanoate ([PR]), and bis(trifluoromethylsulfonyl)imide ([TF₂N]) anions through density functional theory (DFT) simulations is reported. This work is a continuation of a previous work (*J. Phys. Chem. B*, 2014, 118, 11330–11340) wherein the solvation of fullerene C₆₀ by ILs was studied through molecular dynamics simulations. As a first approximation, strong IL···C₆₀ interactions are need to hinder fullerene tendency to the aggregation. Interaction strength was assessed through binding energies between selected ILs and C₆₀ molecule (BE_{IL-C₆₀}). All the selected ILs provided larger BE_{IL-C₆₀} than those previously reported for water···C₆₀ interactions. Likewise, BE_{IL-C₆₀} of some ionic liquids, such as those based on [SA] and [BE] anions, are much larger than BE_{IL-C₆₀} of [BMIM][BF₄] ionic liquids, which would provide adequate features as C₆₀ solvent. The highest binding energies were obtained for [BMIM][SA]. Nonetheless, other ILs also based on [SA] anion displays somewhat lower energies. Therefore, considering the suitable properties of choline and piperazine cations, such as low toxicity, high biodegradability, or low cost, the obtained results infers both [CH][SA] and [MP][MS] ILs as recommended options for C₆₀ solvation and solution.

Aimed at obtaining a deeper understanding of the interaction mechanism at the molecular level, intermolecular interactions (based on topological analysis of the electronic density and RDG isosurfaces) as well as charge distributions were assessed. The IL···C₆₀ interaction mechanism is a mixture of several factors, mainly dispersion interactions, with π – π stacking between [SA] anions and the C₆₀ surface bringing out strong IL···C₆₀ intermolecular bonds. The electronic structure analysis showed that deep HOMO energies (mainly located over the anion) as well as weak interactions between ions would lead to high BE_{IL-C₆₀}.

This work offers fundamental insights into the key parameters governing energetic of IL-C₆₀ systems, providing information for the rational design of ILs as C₆₀ solvents through the adequate cation–anion combinations.

ASSOCIATED CONTENT

Supporting Information

The Supporting Information is available free of charge on the ACS Publications website at DOI: [10.1021/acs.jpcb.5b03608](https://doi.org/10.1021/acs.jpcb.5b03608).

Table 1S (AIM features for those critical points associated with IL···C₆₀ interactions), Figure 1S (charge distribution of IL-C₆₀ systems according Hirshfeld scheme), Figures 2S and 3S (RDG isosurfaces), Figure 4S (density of states of pristine C₆₀), and Figure 5S (frontier orbitals energies) ([PDF](#))

AUTHOR INFORMATION

Corresponding Author

*E-mail: sapar@ubu.es.

Notes

The authors declare no competing financial interest.

ACKNOWLEDGMENTS

This work was made possible by Ministerio de Economía y Competitividad (Spain, project CTQ2013-40476-R) and Junta de Castilla y León (Spain, project BU324U14). Gregorio

García acknowledges the funding by Junta de Castilla y León, co-founded by European Social Fund, for a postdoctoral contract. We also acknowledge The Foundation of Supercomputing Center of Castile and León (FCSCL, Spain), Computing and Advanced Technologies Foundation of Extremadura (CénitS, LUSITANIA Supercomputer, Spain), and Consortium of Scientific and Academic Services of Cataluña (CSUC, Spain) for providing supercomputing facilities. The statements made herein are solely the responsibility of the authors.

REFERENCES

- Kroto, H. W.; Heath, J. R.; O'Brien, S. C.; Curl, R. F.; Smalley, R. E. C₆₀: Buckminsterfullerene. *Nature* 1985, 318, 162–163.
- McHedlov-Petrosyan, N. O. Fullerenes in Liquid Media: An Unsettling Intrusion into the Solution Chemistry. *Chem. Rev.* 2013, 113, 5149–5193.
- Semenov, K. N.; Charykov, N. A.; Keskinov, V. A.; Piartman, A. K.; Blokhin, A. A.; Kopyrin, A. A. Solubility of Light Fullerenes in Organic Solvents. *J. Chem. Eng. Data* 2010, 55, 13–36.
- Wang, C. I.; Hua, C. C.; Chen, S. A. Dynamic Solvation Shell and Solubility of C₆₀ in Organic Solvents. *J. Phys. Chem. B* 2014, 118, 9964–9973.
- Chaban, V.; Maciel, C.; Fileti, E. Does the Like Dissolves Like Rule Hold for Fullerene and Ionic Liquids? *J. Solution Chem.* 2014, 43, 1019–1031.
- Fileti, E. E.; Chaban, V. V. Structure and Supersaturation of Highly Concentrated Solutions of Buckyball in 1-Butyl-3-Methylimidazolium Tetrafluoroborate. *J. Phys. Chem. B* 2014, 118, 7376–7382.
- García, G.; Atilhan, M.; Aparicio, S. Theoretical Study on the Solvation of C₆₀ Fullerene by Ionic Liquids. *J. Phys. Chem. B* 2014, 118, 11330–11340.
- Maciel, C.; Fileti, E. E. Molecular Interactions Between Fullerene C₆₀ and Ionic Liquids. *Chem. Phys. Lett.* 2013, 568–569, 75–79.
- Fileti, E. E.; Chaban, V. V. Imidazolium Ionic Liquid Helps to Disperse Fullerenes in Water. *J. Phys. Chem. Lett.* 2014, 5, 1795–1800.
- Zangi, R. Are Buckyballs Hydrophobic? *J. Phys. Chem. B* 2014, 118, 12263–12270.
- Monticelli, L. On Atomistic and Coarse-Grained Models for C₆₀ Fullerene. *J. Chem. Theory Comput.* 2012, 8, 1370–1378.
- Choi, J. I.; Snow, S. D.; Kim, J.-H.; Jang, S. S. Interaction of C₆₀ with Water: First-Principles Modeling and Environmental Implications. *Environ. Sci. Technol.* 2015, 49, 1529–1536.
- Pourbasheer, E.; Aalizadeh, R.; Ardabili, J. S.; Ganjali, M. R. QSPR Study on Solubility of some Fullerenes Derivatives using the Genetic Algorithms — Multiple Linear Regression. *J. Mol. Liq.* 2015, 204, 162–169.
- Earle-Martyn, J.; Seddon-Kenneth, R. Ionic Liquids: Green Solvents for the Future. In *Clean Solvents*; American Chemical Society, 2002.
- Wilkes, J. S. A short History of Ionic Liquids—from Molten Salts to Neoteric Solvents. *Green Chem.* 2002, 4, 73–80.
- Rogers, R. D.; Seddon, K. R. Ionic Liquids—Solvents of the Future? *Science* 2003, 302, 792–793.
- Lei, Z.; Dai, C.; Chen, B. Gas Solubility in Ionic Liquids. *Chem. Rev.* 2014, 114, 1289–1326.
- Becke, A. D. Density-Functional Thermochemistry. III. The Role of Exact Exchange. *J. Chem. Phys.* 1993, 98, 5648.
- Lee, C.; Yang, W.; Parr, R. G. Development of the Colle-Salvetti Correlation-Energy Formula into a Functional of the Electron Density. *Phys. Rev. B: Condens. Matter Mater. Phys.* 1988, 37, 785–789.
- Becke, A. D. Density-functional Exchange-Energy Approximation with Correct Asymptotic Behavior. *Phys. Rev. A: At., Mol., Opt. Phys.* 1988, 38, 3098–3100.
- Cohen, A. J.; Mori-Sánchez, P.; Yang, W. Challenges for Density Functional Theory. *Chem. Rev.* 2012, 112, 289–320.

- (22) Grimme, S. Semiempirical GGA-type Density Functional Constructed with a Long-Range Dispersion Correction. *J. Comput. Chem.* **2006**, *27*, 1787–1799.
- (23) Schwabe, T.; Grimme, S. Double-Hybrid Density Functionals with Long-Range Dispersion Corrections: Higher Accuracy and Extended Applicability. *Phys. Chem. Chem. Phys.* **2007**, *9*, 3397–3406.
- (24) Simon, S.; Duran, M.; Dannenberg, J. J. How does Basis Set Superposition Error change the Potential Surfaces for Hydrogen-Bonded Dimers? *J. Chem. Phys.* **1996**, *105*, 11024.
- (25) Mulliken, R. S. Electronic Population Analysis on LCAO–MO Molecular Wave Functions. I. *J. Chem. Phys.* **1955**, *23*, 1833.
- (26) Philips, J. J.; Hudspeth, M. A.; Browne, P. M., Jr; Peralta, J. E. Basis Set Dependence of Atomic Spin Populations. *Chem. Phys. Lett.* **2010**, *495*, 146–150.
- (27) Hirshfeld, F. L. Bonded-Atom Fragments for Describing Molecular Charge Densities. *Theoret. Chim. Acta* **1977**, *44*, 129–138.
- (28) Breneman, C. M.; Wiberg, K. B. Determining Atom-Centered Monopoles from Molecular Electrostatic Potentials. The Need for High Sampling Density in Formamide Conformational Analysis. *J. Comput. Chem.* **1990**, *11*, 361–373.
- (29) Aparicio, S.; Atilhan, M. Water Effect on CO₂ Absorption for Hydroxylammonium Based Ionic Liquids: A Molecular Dynamics Study. *Chem. Phys.* **2012**, *400*, 118–125.
- (30) Aparicio, S.; Atilhan, M. Nanoscopic Vision on Fuel Dearomatization Using Ionic Liquids: The Case of Piperazine-Based Fluids. *Energy Fuels* **2013**, *27*, 2515–2527.
- (31) Sanz, V.; Alcalde, R.; Atilhan, M.; Aparicio, S. Insights from Quantum Chemistry into Piperazine-Based Ionic Liquids and Their behavior with Regard to CO₂. *J. Mol. Model.* **2014**, *20*, 1–14.
- (32) Aparicio, S.; Atilhan, M. A Computational Study on Choline Benzoate and Choline Salicylate Ionic Liquids in the Pure State and After CO₂ Adsorption. *J. Phys. Chem. B* **2012**, *116*, 9171–9185.
- (33) Aparicio, S.; Atilhan, M. Computational Study of Hexamethylguanidinium Lactate Ionic Liquid: A Candidate for Natural Gas Sweetening. *Energy Fuels* **2010**, *24*, 4989–5001.
- (34) Bader, R. F. W. *Atoms in Molecules: a Quantum Theory*; Oxford, 1990.
- (35) Johnson, E. R.; Keinan, S.; Mori-Sánchez, P.; Contreras-García, J.; Cohen, A. J.; Yang, W. Revealing Noncovalent Interactions. *J. Am. Chem. Soc.* **2010**, *132*, 6498–6506.
- (36) Frisch, M. J.; Trucks, G. W.; Schlegel, H. B.; Scuseria, G. E.; Robb, M. A.; Cheeseman, J. R.; Scalmani, G.; Barone, V.; Mennucci, B.; Petersson, G. A., et al.. *Gaussian 09*; Gaussian, Inc.: Wallingford, CT, USA, 2009.
- (37) Lu, T.; Chen, F. Multiwfn: A Multifunctional Wavefunction Analyzer. *J. Comput. Chem.* **2012**, *33*, 580–592.
- (38) O'Boyle, N. M.; Tenderholt, A. L.; Langner, K. M. Cclib: A Library for Package-Independent Computational Chemistry Algorithms. *J. Comput. Chem.* **2008**, *29*, 839–845.
- (39) Palusiak, M.; Krygowski, T. M. Application of AIM Parameters at Ring Critical Points for Estimation of π -Electron Delocalization in Six-Membered Aromatic and Quasi-Aromatic Rings. *Chem. - Eur. J.* **2007**, *13*, 7996–8006.
- (40) Couling, D. J.; Bernot, R. J.; Docherty, K. M.; Dixon, J. K.; Maginn, E. J. Assessing the Factors Responsible for Ionic Liquid Toxicity to Aquatic Organisms via Quantitative Structure-Property Relationship Modeling. *Green Chem.* **2006**, *8*, 82–90.
- (41) Lu, X.; Yue, L.; Hu, M.; Cao, Q.; Xu, L.; Guo, Y.; Hu, S.; Fang, W. Piperazinium-Based Ionic Liquids with Lactate Anion for Extractive Desulfurization of Fuels. *Energy Fuels* **2014**, *28*, 1774–1780.